Characterizing Multiscale Variability of Zero Intermittency in Spatial Rainfall

PRAVEEN KUMAR

Universities Space Research Association/Hydrological Sciences Branch, NASA/Goddard Space Flight Center, Greenbelt, Maryland

EFI FOUFOULA-GEORGIOU

St. Anthony Falls Hydraulic Laboratory, Department of Civil and Mineral Engineering, University of Minnesota, Minneapolis, Minnesota

(Manuscript received 20 August 1993, in final form 30 April 1994)

ABSTRACT

In this paper the authors study how zero intermittency in spatial rainfall, as described by the fraction of area covered by rainfall, changes with spatial scale of rainfall measurement or representation. A statistical measure of intermittency that describes the size distribution of "voids" (nonrainy areas imbedded inside rainy areas) as a function of scale is also introduced. Morphological algorithms are proposed for reconstructing rainfall intermittency at fine scales given the intermittency at coarser scales. These algorithms are envisioned to be useful in hydroclimatological studies where the rainfall spatial variability at the subgrid scale needs to be reconstructed from the results of synoptic- or mesoscale meteorological numerical models. The developed methodologies are demonstrated and tested using data from a severe springtime midlatitude squall line and a mild midlatitude winter storm monitored by a meteorological radar in Norman, Oklahoma.

1. Introduction

Rainfall is an intermittent process—that is, nonrainy areas amidst rainy areas continue to exist—for a broad range of spatial and temporal integration scales. Consequently, the distribution of rainfall intensities is of mixed type with an "atom at zero." This feature of rainfall gives rise to unique properties important both for rainfall analysis and measurement. For example, due to rainy areas engulfing nonrainy areas, when the scale increases—that is, resolution decreases—the mean areal rainfall intensity conditioned on being positive, decreases. Also, the fraction of area covered by the storm increases with increasing scale (see, e.g., Figs. 6a and 7a to be discussed later in this paper). The important point to note is that the fraction of area of the viewing window covered by rainfall is a function of the resolution at which rain intensity is represented within the viewing window. This can have important implications in certain hydroclimatology simulation experiments (see Johnson et al. 1991) where the fraction of the area covered by the storm is an important parameter determining the response of the hydrologic system.

Two kinds of climate models use the property of fractional coverage: 1) GCMs (general circulation models) where a storm can lie entirely inside a GCM grid (typically of size 250 km × 250 km) in which case the GCM grid acts like a viewing window; and 2) RCMs (regional climate models or mesoscale models), which have much higher spatial resolution and are capable of resolving the storm in more detail. In this case the mesoscale grid provides the resolution, rather than the viewing window, at which the rainfall is represented. However, in many cases need arises to disaggregate the outputs of these models to still finer resolutions such as in driving a distributed parameter hydrologic model using the output of these climate models. In this paper we develop a methodology for upscaling and downscaling storm area (portion of the viewing window covered by storm) derived from the rain intensities at a certain resolution based on techniques of mathematical morphology. The upscaling (going from small to large scales) is done by a variant of a simple nonlinear morphological operation called dilation. However, the downscaling (going from large to small scales) is more involved. The guiding premise behind the downscaling methodology is the following: since fraction of storm area increases with increasing scale (decreasing resolution), that is, the fraction of voids decreases with increasing scale, the voids should be allowed to *grow* when downscaling. We discuss two algorithms that accomplish this objective in a morphologically consistent manner. They reconstruct intermittency from coarser to finer scales such that the fraction of area covered by rain decreases with increasing resolution. We develop a measure of the statistical nature of intermittency using a probability distribution

Corresponding author address: Dr. Praveen Kumar, Universities Space Research Association, Hydrologic Science Branch, Code 974, NASA/Goddard Space Flight Center, Greenbelt, MD 20771.

© 1994 American Meteorological Society

function that describes the size of voids as a function of scale. One of the algorithms of downscaling storm area relies on this *size distribution function.*

In section 2 the fundamental concepts of morphological operations, to the extent that they are relevant to this research, are reviewed briefly. Detailed presentations can be found in Serra (1982) and Giardina and Dougherty (1988). In section 3 we develop the upscaling algorithm and present the results of morphological analysis on two rainfall datasets: a severe squall-line storm and a winter storm over Norman, Oklahoma. These datasets are described in detail in appendix A. The statistical measure of intermittency, characterized by the size distribution function of voids, is also developed in this section. In section 4 we describe the downscaling algorithms and present some results using the rainfall data.

2. Review of morphological transforms

Morphology is the study of form and structure. The structure of interest to us is the binary field (also called intermittency field) generated by the rainfall intensities; that is, if the rainfall intensities are nonzero then the underlying set is assigned a value of 1 (denoted as Z_1), and zero otherwise (denoted as Z_0). This intermittency field will be denoted as Z; that is, $Z = Z_1 \cup Z_0$. Figures 1 and 2 show the binary fields obtained from frame 1 (see appendix A for definition of "frame") of the squall line and winter storms, respectively.

Morphological operators are nonlinear operators that locally modify the geometrical features of images.

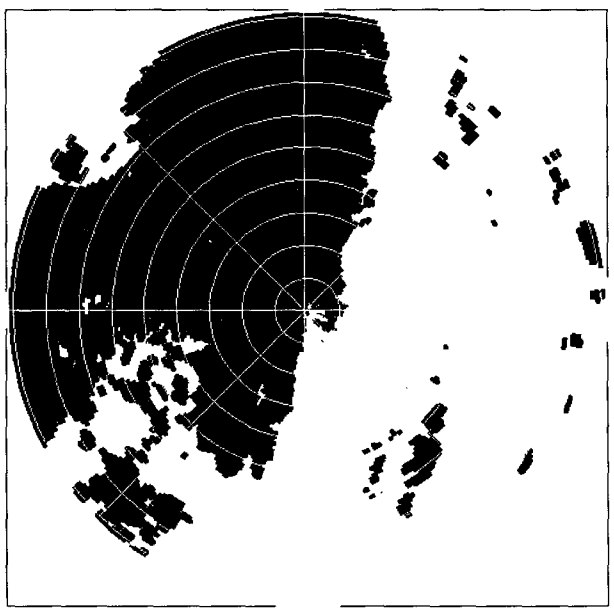

FIG. 1. Binary field obtained from frame 1 of the squall-line storm on a grid of 512 × 512 (relative scale λ = 1). Black represents rainy areas and white represents nonrainy areas. The radial arcs are 25 km apart covering a radius of 230 km.

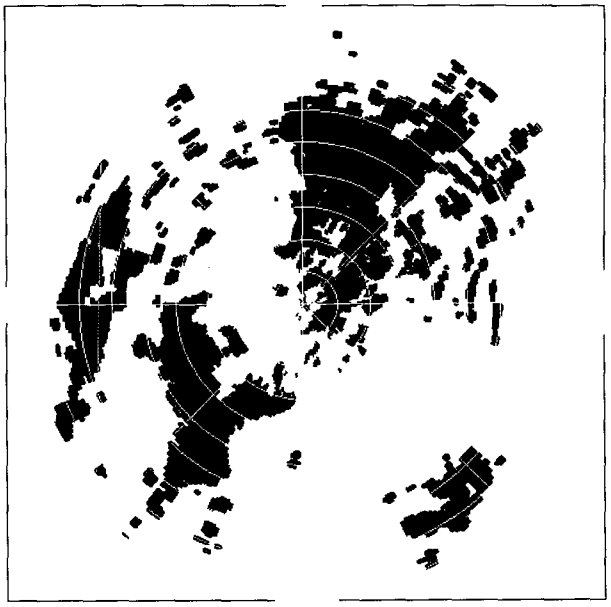

FIG. 2. Same as Fig. 1 for frame 1 of the winter storm. Fraction of area covered by rain is 18.8%.

The morphological operations are defined between two sets **A** and **B** (in the plane), where **A** is the set we wish to study and **B** is called the structuring element. The structuring element **B** plays a role analogous to a kernel in a convolution operation. The fundamental morphological operations are Minkowski addition and subtraction (see Serra 1982). Minkowski addition $\mathbf{A} \oplus \mathbf{B}$ is defined as

$$\mathbf{A} \oplus \mathbf{B} = \bigcup_{b \in \mathbf{B}} \mathbf{A} + b, \tag{1}$$

that is, $\mathbf{A} \oplus \mathbf{B}$ is constructed by translating **A** by each element of **B** and then taking union of all the resulting translates. Minkowski addition is also called (morphological) dilation operation and is written as $\mathbf{D}(\mathbf{A}, \mathbf{B})$ $(=\mathbf{A} \oplus \mathbf{B})$. Minkowski subtraction $\mathbf{A} \ominus \mathbf{B}$ is defined as

$$\mathbf{A} \ominus \mathbf{B} = \bigcap_{b \in \mathbf{B}} \mathbf{A} + b. \tag{2}$$

In this operation, **A** is translated by each element of **B** and then intersection is taken. The operation $\mathbf{A} \ominus (-\mathbf{B})$ is called morphological erosion and is denoted as $\mathbf{E}(\mathbf{A}, \mathbf{B})$ ($-\mathbf{B}$ represents a reflection of **B** about the origin). The result of the erosion operation is the set of translation points such that the translated structuring element **B** is contained within **A**.

Eroding the image by **B** has the effect of shrinking the image in a manner determined by **B**, whereas dilation has the effect of expanding and smoothing the image. Both dilation and erosion are invariant with respect to translation. Although dilation and erosion

are not inverse of each other, they share a *duality* property with respect to complementation given as

$$[\mathbf{D}(\mathbf{A}, \mathbf{B})]' = \mathbf{E}(\mathbf{A}', -\mathbf{B}), \quad (3)$$

$$[\mathbf{E}(\mathbf{A}, \mathbf{B})]' = \mathbf{D}(\mathbf{A}', -\mathbf{B}), \quad (4)$$

where $\mathbf{A}'$ denotes the complement or background of $\mathbf{A}$; that is, $\mathbf{A}' = \{\mathbf{x} : \mathbf{x} \notin \mathbf{A}\}$. In other words, dilation of an image can be accomplished by erosion of the complementary image and vice versa.

Using the basic operations of Minkowski addition and subtraction, more advanced operations called *opening* $[\mathbf{O}(\mathbf{A}, \mathbf{B})]$ and *closing* $[\mathbf{C}(\mathbf{A}, \mathbf{B})]$ can be defined as

$$\mathbf{O}(\mathbf{A}, \mathbf{B}) = [\mathbf{A} \ominus (-\mathbf{B})] \oplus \mathbf{B} = \mathbf{D}(\mathbf{E}(\mathbf{A}, \mathbf{B}), \mathbf{B}) \quad (5)$$

$$\mathbf{C}(\mathbf{A}, \mathbf{B}) = [\mathbf{A} \oplus (-\mathbf{B})] \ominus \mathbf{B} = \mathbf{E}(\mathbf{D}(\mathbf{A}, -\mathbf{B}), -\mathbf{B}), \quad (6)$$

that is, opening is erosion followed by dilation and closing is dilation followed by erosion. The opening and closing operations also satisfy a duality property given as

$$\mathbf{C}(\mathbf{A}, \mathbf{B}) = [\mathbf{O}(\mathbf{A}', \mathbf{B})]' \quad (7)$$

$$\mathbf{O}(\mathbf{A}, \mathbf{B}) = [\mathbf{C}(\mathbf{A}', \mathbf{B})]'; \quad (8)$$

that is, opening of an image can be accomplished by closing of the complementary image and vice versa. The effects of dilation, erosion, opening, and closing operations for an example are shown in Fig. 3 (taken from Giardina and Dougherty 1988). As can be seen from the example, closing has the effect of smoothing an image from the outside by filling thin gulfs and small holes and opening has the effect of smoothing an image from the inside by suppressing the sharp capes and cutting the narrow isthmuses of A in such a way that $\mathbf{O}(\mathbf{A}, \mathbf{B}) \subseteq \mathbf{A} \subseteq \mathbf{C}(\mathbf{A}, \mathbf{B})$. The size and shape of the structuring element determines the nature and degree of smoothing. For algorithms to apply the above morphological operations to digital data, see Giardina and Dougherty (1988).

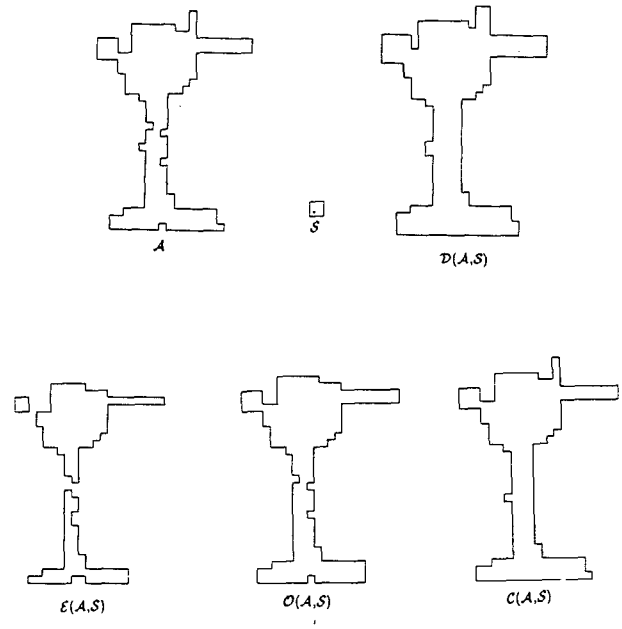

FIG. 3. Illustration of the effect of dilation, erosion, opening, and closing morphological operations on a generic figure.

3. Upscaling and morphological analysis of binary rainfall fields

The objective of this section is to develop a morphological operation that upscales (i.e., decreases resolution of) the binary rainfall intermittency field in a manner that is equivalent to the intermittency field obtained when the rainfall field is scaled by the conventional method of averaging 2×2 nonoverlapping adjacent pixels.

By $\mathbf{S}$, let us denote the structuring element given as

$$\mathbf{S} \equiv \mathbf{S}(\mathbf{x}) = \begin{cases} 1, & \text{if } \mathbf{x} \in [0, 1) \times [0, 1) \\ 0, & \text{otherwise} \end{cases}. \quad (9)$$

Dilating Z by $\mathbf{S}$ and then downsampling every row and column by a factor of 2 (i.e., keeping only alternate pixels in every row and column) gives a binary field that is the same as the binary field obtained from the scaled rainfall field, when this scaling is done by averaging 2×2 nonoverlapping adjacent values. This is due to the fact that the morphological equivalent of averaging 2×2 pixels is the dilation operation where the structuring element is determined by the convolution kernel. Clearly, the structuring element defined above is the appropriate structuring element for 2×2 averaging of pixels. Figure 4 shows the field obtained by morphological dilation of the binary field shown in Fig. 1 using $\mathbf{S}$ and then downsampling by a factor of 2; that is, it depicts $\mathbf{D}(Z_1, \mathbf{S})$ followed by downsampling. Figure 5 shows the binary field corresponding to the scaled rainfall field obtained by averaging nonoverlapping adjacent pixels. The validity of using $\mathbf{S}$ as the structuring element can be seen by comparing Figs. 4 and 5, which are almost identical. The minor differences are because of thresholding error. For example, we use a threshold of 0.01 mm h^{-1} to distinguish between rainy and nonrainy areas. When the rainfall field is averaged to obtain Fig. 5, some pixels that appear rainy at higher resolutions may appear as voids at lower resolution if on averaging the intensity falls below the threshold. Such a situation appears, for example, when a rainy pixel with very low intensity is averaged along with three adjacent nonrainy pixels. This condition, however, does not arise when dilation is performed on the binary field. The dilation can in general be performed at different scales using $\lambda\mathbf{S}$, where $\lambda\mathbf{S}$ denotes λ times dilation of $\mathbf{S}$ with itself—that is, $\mathbf{S} \oplus \mathbf{S} \oplus \cdots \oplus \mathbf{S}$ λ times. We denote this general form of the upscaling operator as U_λ; that is,

FIG. 4. Field obtained after dilation using S and downsampling by a factor of 2 of the binary field obtained from frame 1 of the squall-line storm shown in Fig. 1.

FIG. 5. Binary field obtained by averaging 2×2 nonoverlapping pixels of frame 1 of the squall-line storm.

$$U_\lambda = \mathbf{D}(Z_1, \lambda\mathbf{S})$$

followed by downsampling.

It was indicated in the introduction that an important morphological measure of interest in rainfall modeling is the fraction of total area covered by the storm. Tables 1 and 2 give the values of the fraction of the total area covered, $\vartheta(\lambda)$, with change of scale, for several frames of the squall line and winter storms, respectively, using S as the structuring element. The viewing window is the square enclosing the radar scan area of 230-km radius. Figures 6a and 7a show the plot of these values. For the relation of relative scale λ to physical scale and grid resolution see Table 3.

Because, as scale increases, the fraction of area covered by the storm increases by engulfing nonrainy areas, it is of interest to analyze the morphological properties of these nonrainy areas. The nonrainy areas can be embedded entirely inside rainy areas or they can be on the boundary of rainy areas. The morphological property of interest to us is the *size distribution* of these "voids" (nonrainy area embedded inside rainy area). The probabilistic measure of the size of the voids at scale λ is the cumulative *size distribution function.* The size distribution function of voids, denoted as $\mathbf{G}(\lambda)$, can be defined as

$$\mathbf{G}(\lambda) = \Pr\{\mathbf{x} \in \mathbf{C}(Z_1, \lambda\mathbf{S}) | \mathbf{x} \in Z_0\}; \quad (10)$$

that is, $\mathbf{G}(\lambda)$ represents the probability of a point belonging to the void to belong to the closing of the rainy area, using structuring element S at scale λ. *The size of the void at* x *is the minimum value of* λ *such that* $\mathbf{x} \in \mathbf{C}(Z_1, \lambda\mathbf{S})$ *given* $\mathbf{x} \in Z_0$. In simpler terms, it represents the chance of a void to disappear at the scale λ. The reason for using closing and not dilation in the above definition is given in appendix B.

It can be shown that (see appendix B)

$$\mathbf{G}(\lambda) = \frac{\vartheta_c(\lambda) - \vartheta(1)}{1 - \vartheta(1)}, \quad (11)$$

where

$$\vartheta(1) \equiv \Pr\{\mathbf{x} \in Z_1\}, \quad (12)$$

that is, fraction of the rainy area at the original resolution, and

$$\vartheta_c(\lambda) \equiv \Pr\{\mathbf{x} \in \mathbf{C}(Z_1, \lambda\mathbf{S})\}, \quad (13)$$

that is, fraction of the rainy area after a closing has been performed on Z_1 at scale λ using S as the structuring element. Using the following estimators for $\vartheta(1)$ and $\vartheta_c(\lambda)$:

$$\hat{\vartheta}(1) = \frac{\text{area}(Z_1)}{\text{area}(Z)} \quad (14)$$

and

$$\hat{\vartheta}_c(\lambda) = \frac{\text{area}[\mathbf{C}(Z_1, \lambda\mathbf{S})]}{\text{area}(Z)}, \quad (15)$$

an estimate of $\mathbf{G}(\lambda)$ can be obtained from (11). Area $[\mathbf{C}(Z_1, \lambda\mathbf{S})]$ in the above expression can be alternatively obtained by scaling Z_1, instead of S, using the following equation:

TABLE 1. Values of ϑ, ϑ_c, $\mathbf{G}$, ϑ_D^{16}, and ϑ_D^{32} at different (relative) scales λ for several frames of the squall line dataset.

Time (CST)	Frame	Parameter	$\lambda = 1$	$\lambda = 2$	$\lambda = 4$	$\lambda = 8$	$\lambda = 16$	$\lambda = 32$	$\lambda = 64$
1152–1202	1	ϑ	0.3483	0.3616	0.3847	0.4197	0.4775	0.5820	0.7030
		ϑ_c	0.3500	0.3640	0.3900	0.4290	0.4950	0.6370	0.7500
		$\mathbf{G}$	0.0031	0.0245	0.0644	0.1242	0.2255	0.4433	0.6166
		ϑ_D^{16}	0.3747	0.3813	0.3946	0.4216			
		ϑ_D^{32}	0.4229	0.4280	0.4380	0.4583	0.4990		
1231–1240	5	ϑ	0.3200	0.3334	0.3560	0.3890	0.4434	0.5078	0.6090
		ϑ_c	0.3220	0.3370	0.3620	0.3970	0.4500	0.5350	0.6720
		$\mathbf{G}$	0.0029	0.0250	0.0618	0.1132	0.1912	0.3162	0.5176
		ϑ_D^{16}	0.3754	0.3797	0.3884	0.4036			
		ϑ_D^{32}	0.3865	0.3902	0.3975	0.4126	0.4433		
1319–1329	10	ϑ	0.3754	0.3895	0.4127	0.4500	0.5107	0.6094	0.6880
		ϑ_c	0.3770	0.3920	0.4200	0.4590	0.5330	0.6560	0.7500
		$\mathbf{G}$	0.0032	0.0272	0.0720	0.1344	0.2528	0.4496	0.6000
		ϑ_D^{16}	0.4143	0.4205	0.4329	0.4583			
		ϑ_D^{32}	0.4733	0.4778	0.4868	0.5046	0.5400		
1500–1509	15	ϑ	0.3572	0.3687	0.3883	0.4195	0.4795	0.5625	0.6720
		ϑ_c	0.3580	0.3710	0.3920	0.4260	0.5090	0.5980	0.7500
		$\mathbf{G}$	0.0016	0.0218	0.0544	0.1073	0.2364	0.3748	0.6112
		ϑ_D^{16}	0.3895	0.3952	0.4068	0.4304			
		ϑ_D^{32}	0.4415	0.4455	0.4536	0.4695	0.5010		
1548–1558	20	ϑ	0.3770	0.3920	0.4173	0.4556	0.5205	0.6133	0.6880
		ϑ_c	0.3790	0.3960	0.4240	0.4640	0.5470	0.6600	0.7030
		$\mathbf{G}$	0.0032	0.0305	0.0754	0.1396	0.2729	0.4543	0.5233
		ϑ_D^{16}	0.4252	0.4315	0.4442	0.4695			
		ϑ_D^{32}	0.4960	0.4998	0.5073	0.5225	0.5527		
1637–1646	25	ϑ	0.3900	0.4057	0.4326	0.4763	0.5391	0.6328	0.6720
		ϑ_c	0.3920	0.4090	0.4400	0.4900	0.5650	0.6950	0.7190
		$\mathbf{G}$	0.0033	0.0311	0.0820	0.1639	0.2869	0.5000	0.5393
		ϑ_D^{16}	0.4466	0.4528	0.4651	0.4897			
		ϑ_D^{32}	0.5044	0.5088	0.5175	0.5347	0.5684		

$$\begin{aligned}\mathbf{C}(Z_1, \lambda\mathbf{S}) &= [Z_1 \oplus (-\lambda\mathbf{S})] \ominus (\lambda\mathbf{S}) \\ &= \lambda\left\{\left[\frac{1}{\lambda} Z_1 \oplus (-\mathbf{S})\right] \ominus \mathbf{S}\right\} \\ &= \lambda\mathbf{C}\left(\frac{1}{\lambda} Z_1, \mathbf{S}\right), \end{aligned} \tag{16}$$

where the second equality in the above equation holds due to the linearity of the operations $\oplus$ and $\ominus$. The scaling of Z_1 by any real number α is meant in the usual sense of scaling a field. Tables 1 and 2 list the values of ϑ, ϑ_c, and $\mathbf{G}$ at various relative scales λ for several frames of the two storms using $\mathbf{S}$ as structuring element and Figs. 6b and 7b show the plot of these values on the log–log scale.

The continuous smooth variation of $\mathbf{G}(\lambda)$ versus λ is an indicator that "voids" of all sizes exist within the rainfall field. If "voids" of sizes less than, say $\lambda_{\max}$, existed then $\mathbf{G}(\lambda)$ would achieve a value of unity at $\lambda = \lambda_{\max}$. If voids of distinct sizes $\lambda_1, \lambda_2, \ldots, \lambda_n$ existed then $\mathbf{G}$ would have jumps at these scales. The existence of voids of all sizes is an indicator that the rainfall intermittency field itself is, within appropriate range of scales, in some sense statistically self-similar. More research is required to establish the precise nature of such a self-similarity.

The above methodology easily extends to more general methods of scaling rainfall fields using the wavelet multiresolution framework (see Kumar and Foufoula-Georgiou 1993). In this framework, upscaling is performed using convolution with a finite support function $\Phi(\mathbf{x})$ called the scale function. Recall that the morphological equivalent of convolution is the dilation operation where the structuring element is determined by the convolution kernel. The structuring element $\mathbf{S}_\Phi$ corresponding to the scale function $\Phi(\mathbf{x})$ is obtained by assigning a value of unity to the union of all points that lie within the support of the scale function. The results developed above and in the following sections are valid for the wavelet multiresolution framework if $\mathbf{S}_\Phi$ is used instead of $\mathbf{S}$ as the structuring element.

4. Downscaling rainfall fields

A problem that has become increasingly important in recent hydroclimatological studies is the following.

TABLE 2. Values of ϑ, ϑ_c, $\mathbf{G}$, ϑ_D^{16}, and ϑ_D^{32} at different (relative) scales λ for several frames of the winter storm dataset.

Time (CST)	Frame	Parameter	$\lambda = 1$	$\lambda = 2$	$\lambda = 4$	$\lambda = 8$	$\lambda = 16$	$\lambda = 32$	$\lambda = 64$
1145–1150	1	ϑ	0.1875	0.2085	0.2464	0.3115	0.4100	0.5195	0.6090
		ϑ_c	0.1890	0.2140	0.2570	0.3360	0.4380	0.5860	0.6720
		$\mathbf{G}$	0.0012	0.0320	0.0850	0.1823	0.3079	0.4901	0.5961
		ϑ_D^{16}	0.2901	0.2981	0.3140	0.3459			
		ϑ_D^{32}	0.3459	0.3520	0.3640	0.3877	0.4336		
1206–1210	5	ϑ	0.2230	0.2436	0.2809	0.3398	0.4277	0.5547	0.6250
		ϑ_c	0.2250	0.2490	0.2920	0.3590	0.4520	0.6130	0.6720
		$\mathbf{G}$	0.0026	0.0335	0.0888	0.1750	0.2947	0.5019	0.5779
		ϑ_D^{16}	0.3142	0.3217	0.3367	0.3669			
		ϑ_D^{32}	0.4187	0.4233	0.4325	0.4507	0.4863		
1241–1247	10	ϑ	0.1967	0.2148	0.2463	0.3003	0.3857	0.5078	0.5780
		ϑ_c	0.1980	0.2190	0.2540	0.3170	0.4060	0.5740	0.5940
		$\mathbf{G}$	0.0012	0.0274	0.0710	0.1494	0.2603	0.4695	0.4944
		ϑ_D^{16}	0.2649	0.2731	0.2892	0.3215			
		ϑ_D^{32}	0.3492	0.3547	0.3655	0.3870	0.4287		
1308–1313	15	ϑ	0.1728	0.1891	0.2171	0.2668	0.3457	0.4726	0.5630
		ϑ_c	0.1740	0.1920	0.2240	0.2820	0.3710	0.5200	0.6100
		$\mathbf{G}$	0.0012	0.0230	0.0617	0.1318	0.2394	0.4196	0.5284
		ϑ_D^{16}	0.2275	0.2354	0.2510	0.2825			
		ϑ_D^{32}	0.3216	0.3268	0.3372	0.3577	0.3975		
1340–1346	20	ϑ	0.1283	0.1420	0.1665	0.2100	0.2734	0.3828	0.5000
		ϑ_c	0.1300	0.1450	0.1730	0.2200	0.3010	0.4340	0.6100
		$\mathbf{G}$	0.0023	0.0195	0.0516	0.1055	0.1984	0.3509	0.5528
		ϑ_D^{16}	0.1687	0.1754	0.1888	0.2163			
		ϑ_D^{32}	0.2386	0.2432	0.2521	0.2700	0.3066		
1410–1416	25	ϑ	0.1290	0.1398	0.1603	0.1975	0.2686	0.3711	0.4690
		ϑ_c	0.1298	0.1420	0.1640	0.2070	0.2970	0.4020	0.5470
		$\mathbf{G}$	0.0010	0.0150	0.0403	0.0897	0.1930	0.3135	0.4800
		ϑ_D^{16}	0.1621	0.1690	0.1829	0.2109			
		ϑ_D^{32}	0.2198	0.2248	0.2348	0.2546	0.2939		

Suppose we are given rainfall intensities at a coarse grid. How should we disaggregate these values to obtain an intensity field at a finer scale (higher resolution)? Such a problem, for example, arises when the output of a mesoscale atmospheric model or general circulation model (which is at a larger scale) is used to drive a regional hydrologic model (at much smaller scale). This problem of subgrid-scale disaggregation has three, not necessarily independent, aspects to it—namely, meteorological, statistical, and morphological. Here we discuss the morphological aspects only and present evidence that they relate to meteorology through the dependence of the size distribution function to storm type. Statistical aspects related to the spatial distribution of nonrainy areas at different scales are not discussed.

Recognizing, from the analysis of the previous section, that the fraction of area covered by rain is much larger when computed at a large scale than at a small scale, we need to find an algorithm that will appropriately decrease the fraction of area covered when we go from a large scale to a small scale (low to high resolution). Within the rainfall intensity itself, there is no statistical information that will help us accomplish this objective. However, the morphological information can be useful. For example, a void within or at the boundary of the rainy area at a large scale can be thought to have been left over from an even larger void at the finer scale. Therefore, an inverse algorithm should allow these voids to grow when the resolution increases. This approach is markedly different from those currently adopted, which assign a rainfall value to all points on the finer grid that fall within a coarser grid that has a positive rainfall value. Such an approach implicitly assumes that the fraction of area covered by rainfall remains constant with change in scale, an assumption that is far from reality as seen from the results of the previous section. Figure 8 shows the binary rainfall field (at grid 512×512, defined as $\lambda = 1$) obtained using this traditional algorithm from a grid at a resolution 2^4 times smaller than that shown in Fig. 2 (i.e., from a grid of 32×32) for the winter storm. As is evident the fraction of area covered is significantly larger than that at finest resolution shown in Fig. 2 (41.0% as compared to 18.8%, see Table 2). All computations are performed with respect to the 512×512 rectangular grid that encloses the circular radar scan

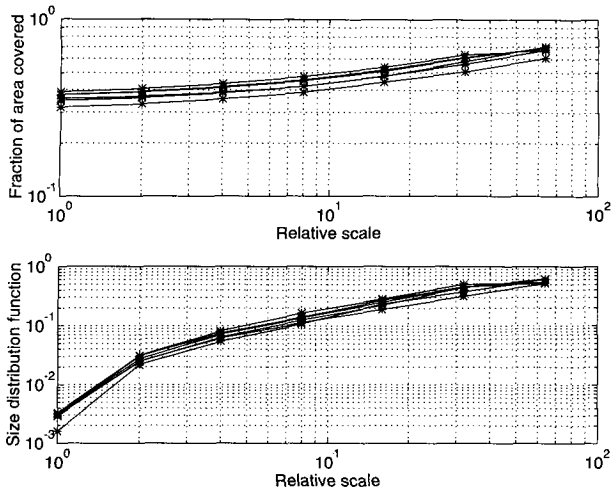

FIG. 6. Variation of (a) fraction of area covered ϑ and (b) size distribution function **G** with respect to relative scale λ for several frames of the squall-line dataset.

area of radius 230 km. No correction is made for the increased area of voids since all structuring elements that are defined are squares and any correction applied would not be consistent across scales. However, this does not change the interpretation of the results.

A heuristic algorithm we propose to use to go from a large scale to the next smaller scale (downscaling) is to upsample every row and column by a factor of 2 and perform a closing operation, and recursively continue this procedure from the largest scale to the desired smallest scale. We denote this operation as D_λ; that is, D_λ is the upsampling followed by $\mathbf{C}(Z_1, \lambda\mathbf{S})$. Upsampling entails inserting a zero between every row and column.

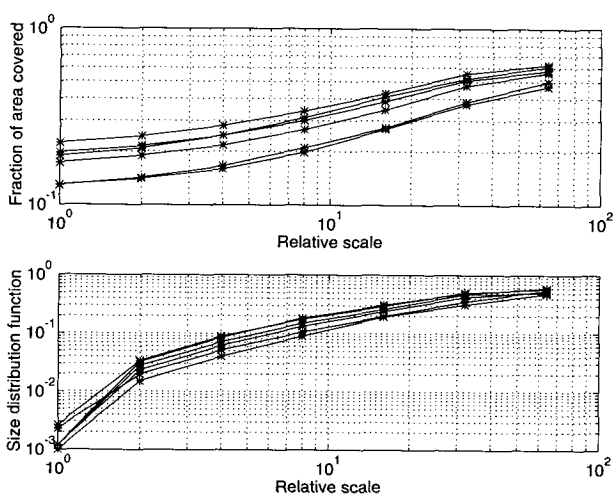

FIG. 7. Variation of (a) fraction of area covered ϑ and (b) size distribution function **G** with respect to relative scale λ for several frames of the winter storm dataset.

TABLE 3. Relationship between relative scale, grid resolution, and physical scale.

Relative scale (linear) λ	Grid (resolution)	Physical scale (km^2)
1	512 × 512	0.898 × 0.898
2	256 × 256	1.797 × 1.797
4	128 × 128	3.594 × 3.594
8	64 × 64	7.188 × 7.188
16	32 × 32	14.375 × 14.375
32	16 × 16	28.75 × 28.75
64	8 × 8	57.5 × 57.5
128	4 × 4	115 × 115

Given the field at some large scale λ_0, we can recursively construct the field at smaller scales λ ($<\lambda_0$) using the above algorithm. Let $\vartheta_D^{\lambda_0}(\lambda)$ denote the fraction of area covered at scale λ ($<\lambda_0$) when the above algorithm, that is, operator D_λ, is initiated at scale λ_0. Tables 1 and 2 give the values of this parameter for several frames for $\lambda_0 = 16$ and $\lambda_0 = 32$ for the squall line and winter storm, respectively. As an illustration, Fig. 9 shows the binary rainfall field at $\lambda = 1$ for the winter storm obtained using this algorithm starting at $\lambda_0 = 16$ (grid of 32 × 32). The structuring element used is **S**. The fraction of area covered (29.0%) is remarkably smaller than that of the field obtained by assuming a constant fraction of area covered by rain (41%, shown in Fig. 8) and the storm area obtained is similar to the original storm area (shown in Fig. 2).

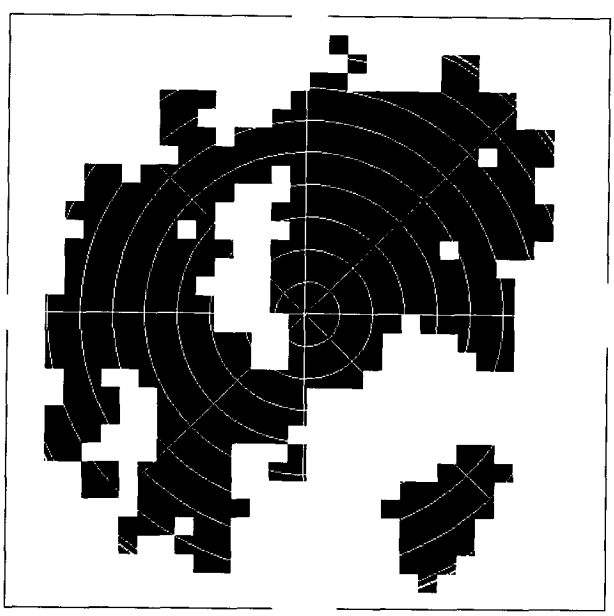

FIG. 8. Binary field on a grid of 512 × 512 (relative scale $\lambda = 1$) obtained by enlarging the field on a grid 32 × 32 (relative scale $\lambda = 16$) for frame 1 of the winter storm. Fraction of area covered by rain is 41%.

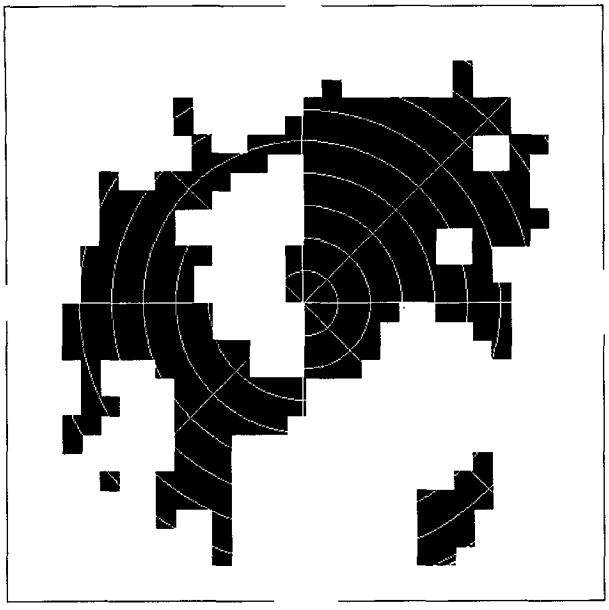

FIG. 9. Binary field at grid of 512 × 512 (relative scale $\lambda = 1$) obtained by recursively upsampling and (morphologically) closing the field at grid 32 × 32 (relative scale $\lambda = 16$) for frame 1 of the winter storm. Fraction of area covered by rain is 29%.

It can be seen by studying Tables 1 and 2 that the larger the value of λ_0—that is, the larger the scale at which we initiate the algorithm—the larger the difference $\vartheta_D^{\lambda_0}(1) - \vartheta(1)$—that is, the difference between the reconstructed and actual fraction of area covered by storm. This is because voids of size less than λ_0 do not "survive" at scale λ_0, and consequently the algorithm is unable to account for such voids. It is possible to make an estimate of this difference $\vartheta_D^{\lambda_0}(1) - \vartheta(1)$ using the size distribution function $\mathbf{G}(\lambda)$. It is easy to see that since $[1 - \vartheta(1)]$ gives the fraction of voids at the unit scale, $[1 - \vartheta(1)]\mathbf{G}(\lambda_0/2)$ is the fraction of voids "engulfed" by the rainy area up to scale λ_0 (we use $\lambda_0/2$ in the above product because our scales increase or decrease as powers of 2 and consequently $\lambda_0/2$ is the next lower scale to λ_0). Hence,

$$\vartheta_D^{\lambda_0}(1) + \mathbf{G}\left(\frac{\lambda_0}{2}\right)[1 - \vartheta(1)] \approx \vartheta(\lambda_0). \quad (17)$$

In this expression the approximation is because we use closing or opening in the definition of size distribution function (to be mathematically consistent), whereas $\vartheta(\lambda)$ is obtained using dilations. The approximation error, however, is small as illustrated below. We define the lhs of the expression (17) as $\vartheta_{DG}(\lambda_0)$; that is, $\vartheta_{DG}(\lambda_0) \equiv \vartheta_D^{\lambda_0}(1) + \mathbf{G}(\lambda_0/2)[1 - \vartheta(1)]$. Table 4 gives the values of $\vartheta_{DG}(\lambda_0)$, $\vartheta(\lambda_0)$, and the percentage approximation error for several frames for the squall line and the winter storms, respectively. As can be seen from these results, the size distribution function, $\mathbf{G}(\lambda)$, is able to account for the voids at different scales fairly well, although on the average the error increases with increasing λ_0. As mentioned earlier, the discrepancy is due to the use of opening or closing in the size distribution function. One could, for heuristic reasons, use erosion or dilation as the basis to define the size distribution function but that will not yield a true size distribution function (see appendix B).

To improve the performance of our downscaling algorithm, we need to statistically incorporate voids at various scales λ ($<\lambda_0$) as we recursively implement the operator D_λ for scales λ_0 to unity. We call this modified operator—that is, D_λ coupled with size distribution function—as $D_{G(\lambda)}$. Therefore, $D_{G(\lambda)}$ is the upsampling followed by $\mathbf{C}(Z_1, \lambda\mathbf{S})$ coupled with $\mathbf{G}(\lambda)$. This improved algorithm can be implemented by developing a spatial distribution model (e.g., Poisson or possibly clustered models) for distribution of voids at different

TABLE 4. Values of $\vartheta(\lambda_0)$ and $\vartheta_{DG}(\lambda_0)$ and their discrepancy error for several frames of the squall line and winter storm.

		Squall line			Winter storm		
Frame	λ_0	$\vartheta(\lambda_0)$	$\vartheta_{DG}(\lambda_0)$	Percent error	$\vartheta(\lambda_0)$	$\vartheta_{DG}(\lambda_0)$	Percent error
1	16	0.4775	0.4556	4.59	0.4100	0.4382	−6.88
	32	0.5820	0.5699	2.08	0.5195	0.5961	14.74
5	16	0.4434	0.4523	−2.01	0.4770	0.4502	5.62
	32	0.5078	0.5165	1.71	0.5547	0.6477	−16.76
10	16	0.5107	0.4982	2.45	0.3857	0.3849	0.21
	32	0.6094	0.6312	−3.58	0.5078	0.5583	−9.94
15	16	0.4795	0.4584	4.40	0.3457	0.3365	2.66
	32	0.5625	0.5935	−5.51	0.4726	0.5196	−9.94
20	16	0.5205	0.5122	1.59	0.2734	0.2607	4.65
	32	0.6133	0.6660	−8.59	0.3828	0.4115	−7.50
25	16	0.5391	0.5466	−1.39	0.2686	0.2402	10.57
	32	0.6328	0.6794	−7.36	0.3711	0.3879	−4.53

scales [characterized by $\mathbf{G}(\lambda)$]. Such an algorithm would require a parameterization of the size distribution function $\mathbf{G}(\lambda)$ that can be obtained either by extensive analysis of many storms or by physical parameterization. Such a study is currently under investigation.

5. Conclusions

Zero intermittency in spatial rainfall varies considerably with the scale at which rainfall is represented. The fraction of area covered by rainfall (ϑ), which is a common measure of intermittency, increases with increasing scale λ at a rate that depends on the type of storm. For example, for the squall-line storm analyzed, ϑ changes from approximately 0.3 to 0.7 over spatial integration scales of approximately 1×1 to 55×55 km^2. For the winter-type storm this change is more dramatic from 0.1 to 0.7 (see Fig. 7). The reason for this change is that voids tend to disappear as the integration scale increases. A probabilistic measure of this change [size distribution function of voids, $\mathbf{G}(\lambda)$] was introduced and was computed for the two storms analyzed. It was found that this function is very similar for both storms and its continuous nature reveals that voids of all sizes exist in the storm area.

The objective of this paper was to develop a morphologically based algorithm for reconstructing rainfall intermittency across scales, that is, upscaling (going from small scales to larger scales) and downscaling (going from large scales to smaller scales). The upscaling algorithm was developed to produce a binary field that is consistent with that obtained from the scaled rainfall field. Two algorithms were developed to downscale storm area. The first downscaling algorithm attempts to reduce the fraction of area covered using the morphology of the storm area at the large scale. The second further improves the first algorithm by incorporating the size distribution function. These algorithms are envisioned to be useful in subgrid-scale disaggregation applications, which are of significant importance in hydroclimatological modeling.

To address the subgrid-scale disaggregation of rainfall we need to specifically address three issues, namely, meteorological, statistical, and morphological. Although, the morphological algorithms developed in this work give a handle on subgrid-scale disaggregation (downscaling) of storm area, they have to be carefully coupled with the other two aspects. For example, while reducing the fraction of area covered while downscaling, the rain intensities need to be redistributed from the larger area to the smaller area, satisfying certain performance criteria such as preservation of total rainfall volume. Recognizing that although the mean rainfall changes with scale, it changes in a manner that the total amount of rainfall volume does not change with scale; one can use this as a criterion while redistributing rain intensities. Such issues are currently under investigation.

APPENDIX A

Description of Radar Rainfall Data

The storms used in this analysis are a squall-line storm and a winter rainstorm that occurred over Norman, Oklahoma. The squall-line storm occurred on 17 May 1987 and the winter storm on 22 February 1985. These storms were monitored by the National Severe Storm Laboratory (NSSL) using a WSR-57 radar that is a 10-cm-wavelength system with a peak power of 305 kW and a beamwidth of 2.2°. The conversion of the cloud reflectivity (dBZ) to rainfall rates (mm h^{-1}) was done at NSSL in Norman, Oklahoma, using the relationship $Z = 300R^{1.4}$, where R is rainfall rate (mm h^{-1}) and the reflectivity factor dBZ is related to Z (mm^6 m^{-3}) by the relationship 1 dBZ = 10 log$Z$. The rainfall intensity values for the squall-line storm are available at a temporal integration scale of 10 min, for 360 azimuths, with every azimuth containing 115 estimates for a range of 230 km (i.e., data at every 2 km × 1°). The data for the winter storm are available at temporal integration scales of 5 min at the same spatial resolution. Data for each time integration scales (10 min for squall line and 5 min for winter rainstorm) over the 360 azimuths are referred to as a "frame." The *precipitation processing system,* used to correlate reflectivity and rainfall intensity, taking into account the rain gauge observations, and adjustment for ground clutter, etc., is described by O'Bannon and Ahnert (1986). For the purpose of our analysis the original data were converted to a rectangular grid lattice of size 512×512 by bilinear interpolation on the polar grid. All results are with respect to this interpolated data.

APPENDIX B

Derivation of $\mathbf{G}(\lambda)$

To define a measure of the *size distribution* of voids, a morphological *size operator* needs to be developed. An operator Υ acting on an image $\mathbf{A}$ at scale (or size) λ [denoted as $\Upsilon_\lambda(\mathbf{A})$] needs to satisfy the following axiomatic properties, originally developed by Matheron, to qualify as a size operator (see Serra 1982, chapter X):

1) $\Upsilon_\lambda(\mathbf{A}) \subset \mathbf{A} \quad \forall \lambda > 0;$

that is, features larger than λ are a subset of the original image.

2) If $\mathbf{B} \subset \mathbf{A}$ the $\Upsilon_\lambda(\mathbf{B}) \subset \Upsilon_\lambda(\mathbf{A}) \quad \forall \lambda \geq 0;$

that is, Υ is an increasing transformation.

3) $\Upsilon_{\lambda_1}[\Upsilon_{\lambda_2}(\mathbf{A})] = \Upsilon_{\lambda_2}[\Upsilon_{\lambda_1}(\mathbf{A})] = \Upsilon_{\max(\lambda_1,\lambda_2)}(\mathbf{A}) \quad \forall \lambda_1, \lambda_2 > 0.$

4) $\Upsilon_\lambda(\mathbf{A} + \mathbf{x}) = \Upsilon_\lambda(\mathbf{A}) \quad \mathbf{x} \in \mathbf{R}^2;$

that is, the size operator is translation invariant. A sizing criterion is a criterion that satisfies the above four axioms. It can be shown that every morphological size distribution operation is a union of (morphological) openings using structuring elements that have convex shape and are compact (see Serra 1982).

To study the size distribution we use the cumulative size distribution function $\mathbf{G_O}(\lambda)$, which specifies the proportion of the points $\mathbf{x} \in \mathbf{A}$ that have been eliminated by the structuring element $\lambda\mathbf{B}$:

$$\mathbf{G_O}(\lambda) = \Pr\{\mathbf{x} \notin \mathbf{O}(\mathbf{A}, \lambda\mathbf{B}) | \mathbf{x} \in \mathbf{A}\} \quad \lambda > 0 \tag{B1}$$

$$= 1 - \Pr\{\mathbf{x} \in \mathbf{O}(\mathbf{A}, \lambda\mathbf{B}) | \mathbf{x} \in \mathbf{A}\} \tag{B2}$$

$$= 1 - \frac{\Pr\{\mathbf{x} \in \mathbf{O}(\mathbf{A}, \lambda\mathbf{B}) \text{ and } \mathbf{x} \in \mathbf{A}\}}{\Pr\{\mathbf{x} \in \mathbf{A}\}}. \tag{B3}$$

But $\Pr\{\mathbf{x} \in \mathbf{O}(\mathbf{A}, \lambda\mathbf{B}) \text{ and } \mathbf{x} \in \mathbf{A}\}$ is the same as $\Pr\{\mathbf{x} \in \mathbf{O}(\mathbf{A}, \lambda\mathbf{B})\}$ since $\mathbf{O}(\mathbf{A}, \lambda\mathbf{B}) \subset \mathbf{A}$ (see Serra 1982, p. 52), and therefore

$$\mathbf{G_O}(\lambda) = 1 - \frac{\Pr\{\mathbf{x} \in \mathbf{O}(\mathbf{A}, \lambda\mathbf{B})\}}{\Pr\{\mathbf{x} \in \mathbf{A}\}}. \tag{B4}$$

Similarly, we can derive an expression for the cumulative size distribution $\mathbf{G}(\lambda)$ of the complementary field $\mathbf{A}'$:

$$\mathbf{G}(\lambda) = \Pr\{\mathbf{x} \notin \mathbf{O}(\mathbf{A}', \lambda\mathbf{B}) | \mathbf{x} \in \mathbf{A}'\}. \tag{B5}$$

Using Eq. (8) we get

$$\mathbf{G}(\lambda) = \Pr\{\mathbf{x} \in \mathbf{C}(\mathbf{A}, \lambda\mathbf{B}) | \mathbf{x} \in \mathbf{A}'\} \tag{B6}$$

$$= \frac{\Pr\{\mathbf{x} \in \mathbf{C}(\mathbf{A}, \lambda\mathbf{B}) \text{ and } \mathbf{x} \in \mathbf{A}'\}}{\Pr\{\mathbf{x} \in \mathbf{A}'\}}. \tag{B7}$$

Using the property that if $\mathbf{A}_1 \subset \mathbf{A}$ then $\mathbf{C}(\mathbf{A}_1, \mathbf{B}) \supset \mathbf{C}(\mathbf{A}, \mathbf{B})$ (see Serra 1982, p. 52) we can further simplify the above expression to get

$$\mathbf{G}(\lambda) = \frac{\Pr\{\mathbf{x} \in \mathbf{C}(\mathbf{A}, \lambda\mathbf{B})\} - \Pr\{\mathbf{x} \in \mathbf{A}\}}{1 - \Pr\{\mathbf{x} \in \mathbf{A}\}}. \tag{B8}$$

The size distribution of the complementary image can be obtained in terms of the closing operation on the original image due to the duality of the two operations.

We can use Eq. (B4) for size distribution of the rainy areas, Z_1, and Eq. (B8) for the voids in the rainy areas. Our main interest will be in the nature of $\mathbf{G}(\lambda)$. For the field Z we use the following estimators for the various probabilities in the above expressions:

$$\Pr\{\mathbf{x} \in \mathbf{Z}_1\} \equiv \vartheta(1) = \frac{\text{area}(Z_1)}{\text{area}(Z)}; \tag{B9}$$

that is, fraction of the rainy area at the original resolution.

$$\Pr\{\mathbf{x} \in \mathbf{O}(Z_1, \lambda\mathbf{S})\}$$

$$\equiv \vartheta_o(\lambda) = \frac{\text{area}[\mathbf{O}(Z_1, \lambda\mathbf{S})]}{\text{area}(Z)}; \tag{B10}$$

that is, fraction of the rainy area after an opening has been performed on Z_1 at scale λ using $\mathbf{S}$.

$$\Pr\{\mathbf{x} \in \mathbf{C}(Z_1, \lambda\mathbf{S})\}$$

$$\equiv \vartheta_c(\lambda) = \frac{\text{area}[\mathbf{C}(Z_1, \lambda\mathbf{S})]}{\text{area}(Z)}; \tag{B11}$$

that is, fraction of the rainy area after a closing has been performed on Z_1 at scale λ using $\mathbf{S}$. Therefore, for the rainfall process, Eqs. (B4) and (B8) reduce to

$$\mathbf{G_O}(\lambda) = 1 - \frac{\vartheta_o(\lambda)}{\vartheta(1)} \tag{B12}$$

and

$$\mathbf{G}(\lambda) = \frac{\vartheta_c(\lambda) - \vartheta(1)}{1 - \vartheta(1)}. \tag{B13}$$

Acknowledgments. This research was supported in part by National Science Foundation Grants BSC-8957469 and EAR-9117866, NASA Grant NAG 5-2108, and a NASA Graduate Student Fellowship for Global Change Research. We thank Tim O'Bannon of NEXRAD Operational Support Facility, Norman, Oklahoma, for providing us with the rainfall data.

REFERENCES

Giardina, C. R., and E. R. Dougherty, 1988: *Morphological Methods in Image and Signal Processing.* Prentice Hall, 321 pp.

Johnson, K. D., D. Entekhabi, and P. S. Eagleson, 1991: The implementation and validation of improved land surface hydrology in an atmospheric general circulation model. Rep. No. 334, Ralph M. Parsons Laboratory, Massachusetts Institute of Technology, 220 pp.

Kumar, P., and E. Foufoula-Georgiou, 1993: A multicomponent decomposition of spatial rainfall fields: 1. Segregation of large and small scale features using wavelet transforms. *Water Resour. Res.*, **29**, 2515–2532.

O'Bannon, T., and P. Ahnert, 1986: A study of the NEXRAD precipitation processing system on a winter-type Oklahoma rainstorm. *Proc. 23d Conf. on Radar Meteorology and the Conf. on Cloud Physics,* Snowmass, CO, Amer. Meteor. Soc., JP99–JP102.

Serra, J., 1982: *Image Analysis and Mathematical Morphology.* Academic Press, 610 pp.